Journal of Computer Assisted Tomography
25(4):515–519

High *b*-Value Diffusion-Weighted MRI of Normal Brain

Jonathan H. Burdette, David D. Durden, Allen D. Elster, and Yi-Fen Yen

Purpose: As MR scanner hardware has improved, allowing for increased gradient strengths, we are able to generate higher *b* values for diffusion-weighted (DW) imaging. Our purpose was to evaluate the appearance of the normal brain on DW MR images as the diffusion gradient strength ("*b* value") is increased from 1,000 to 3,000 s/mm^2.

Method: Three sets of echo planar images were acquired at 1.5 T in 25 normal subjects (mean age 61 years) using progressively increasing strengths of a diffusion-sensitizing gradient (corresponding to *b* values of 0, 1,000, and 3,000 s/mm^2). All other imaging parameters remained constant. Qualitative assessments of trace images were performed by two neuroradiologists, supplemented by quantitative measures of MR signal and noise in eight different anatomic regions.

Results: As gradient strength increased from $b = 1{,}000$ to 3,000, both gray and white matter structures diminished in signal as expected based on their relative diffusion coefficients [calculated average apparent diffusion coefficient (ADC) values: gray matter $= 8.5 \times 10^{-4}$ mm^2/s, white matter $= 7.5 \times 10^{-4}$ mm^2/s]. The signal-to-noise ratios for the $b = 1{,}000$ images were approximately 2.2 times higher than for the $b = 3{,}000$ images ($p < 0.0001$). As the strength of the diffusion-sensitizing gradient increased, white matter became progressively hyperintense to gray matter. Relative to the thalamus, for example, the average MR signal intensity of white matter structures increased by an average of 27.5%, with the densely packed white matter tracts (e.g., middle cerebellar peduncle, tegmentum, and internal capsule) increasing the most.

Conclusion: Brain DW images obtained at $b = 3{,}000$ appear significantly different from those obtained at $b = 1{,}000$, reflecting expected loss of signal from all areas of brain in proportion to their ADC values. Consequently, when all other imaging parameters are held constant, $b = 3{,}000$ DW images appear significantly noisier than $b = 1{,}000$ images, and white matter tracts are significantly more hyperintense than gray matter structures.

Index Terms: Magnetic resonance imaging—Magnetic resonance imaging, techniques—Brain.

Diffusion-weighted (DW) magnetic resonance (MR) brain imaging has become an important component of the modern imaging armamentarium, using powerful gradients coupled with rapid data acquisition to accentuate phase shifts between protons with different rates of diffusion. Contrast in the resulting DW image is derived principally from a combination of T2 and apparent diffusion coefficient (ADC) effects (1,2). The relative degree of diffusion weighting is a function of the "*b* value," which in turn depends on the strength and timing of the diffusion-sensitizing gradients (3).

Almost all DW imaging studies published to date have used *b* values of ≤1,200 s/mm^2 (4–21). Recently, however, more powerful gradients have become commercially available, allowing the generation of DW images with *b* values of ≥3,000 s/mm^2. In our preliminary experience, we noted that higher *b*-value brain images demonstrated several features and properties not well appreciated at lower *b* values. We therefore set out to systematically study and analyze the differences between $b = 1{,}000$ and $b = 3{,}000$ DW brain images in a set of normal subjects.

METHODS

Our study population comprised 25 patients and volunteers (with institutional review board approval)

From the Departments of Radiology (J. H. Burdette, D. D. Durden, and A. D. Elster) and Medical Engineering (Y.-F. Yen), Wake Forest University School of Medicine, Bowman Gray Campus, Winston-Salem, NC, U.S.A.

Address correspondence and reprint requests to Dr. J. H. Burdette at Department of Radiology, Wake Forest University School of Medicine, Bowman Gray Campus, Medical Center Boulevard, Winston-Salem, NC 27157, U.S.A. E-mail: jburdett@wfubmc.edu

referred for MRI over a 3 month period whose routine brain MR images were interpreted as "within normal limits for age" by two board-certified neuroradiologists. The population consisted of 11 men and 14 women, ranging in age from 32 to 86 years, with a mean age of 61 years. All examinations were performed at 1.5 T on a commercially available MR scanner (Echo-Speed LX; GE Medical Systems, Milwaukee, WI, U.S.A.) equipped with high performance gradients of maximum strength 40 mT/m and slew rate of 150 T/m/s.

For each patient, single-shot spin-echo echo-planar imaging was performed in the axial plane using progressively increasing strengths of a tridirectional diffusion-sensitizing gradient (corresponding to b values of 0, 1,000, and 3,000 s/mm^2). All other imaging parameters remained constant (TR = 10,000 ms, TE_{eff} = 97 ms, FOV = 24 cm, 128 × 192 matrix, thickness = 5 mm, NEX = 2). The b = 1,000 and b = 3,000 data sets were displayed as trace DW images, averaging information obtained during sequential activation of the x-, y-, and z-axis diffusion-sensitizing gradients.

The two neuroradiologists jointly performed qualitative evaluations of the b = 0, b = 1,000, and b = 3,000 image sets on all subjects. Thereafter, quantitative region-of-interest measurements of MR signal and noise were obtained in eight anatomic brain regions: posterior limb of the internal capsule, frontal lobe white matter, cerebral peduncle, tegmentum, thalamus, parietal gray matter, cerebellar hemisphere, and middle cerebellar peduncle. All measurements were performed in the left cerebral hemisphere of each subject. From these measurements, MR signal ratios of each anatomic area relative to thalamus and signal-to-noise-ratios (SNRs) were calculated. The ADC of each area was also computed with a two point regression technique using the b = 0 and b = 1,000 images (22,23). Statistical analysis was performed using data tools in Excel for Windows 2000 (Microsoft, Redmond, WA, U.S.A.).

RESULTS

As gradient strength increased from b = 1,000 to 3,000, both gray and white matter structures diminished in signal intensity as expected based on their relative diffusion coefficients (Table 1). Averaging results from five white matter and two gray matter structures, we calculated the ADC value of white matter and gray matter to be approximately 7.5×10^{-4} and 8.5×10^{-4} mm^2/s, respectively, and as low as 7.0×10^{-4} mm^2/s in the posterior limb of the internal capsule. As a result of this gray matter-white matter differential, as the b value is increased, gray matter decreased in signal intensity rapidly and white matter became relatively hyperintense. We considered the cerebellar hemisphere to be a mixture of gray matter and white matter structures, and the calculated ADC value was 7.3×10^{-4} mm^2/s, a value most similar to white matter, accounting for the relatively hyperintense appearance of the cerebellum on the b = 3,000 images.

When no diffusion-sensitizing gradients were used (b = 0), white matter was generally significantly hypointense compared with gray matter on the T2-weighted echo planar images (Fig. 1). When diffusion gradients were raised to the b = 1,000 level, white matter increased in signal relative to gray matter but still remained slightly hypointense. On b = 3,000 images, most white matter tracts were significantly hyperintense relative to cortex and deep gray matter structures.

Region-of-interest signal measurements substantiated these visually apparent observations. Figure 2 displays in graphical form average calculated signal ratios (normalized to thalamic signal) for both b values. Reflecting differences in ADCs, the normalized b = 1,000 and 3,000 signals ranged from 1.12 and 1.08 in the parietal gray matter to 1.20 and 1.54 in the posterior limb of the internal capsule.

In general, the b = 3,000 images appeared "noisier" when compared with the b = 1,000 images, a trend confirmed quantitatively (Fig. 3). As expected, the SNR at b = 1,000 was significantly larger ($p < 0.0001$) than at b = 3,000. For all regions analyzed, the average SNR was 26 ± 4.2 and 12 ± 2.2 for b = 1,000 and 3,000, respectively.

DISCUSSION

DW imaging has become a vital component in the evaluation of the brain by MR, particularly in the setting

TABLE 1. *Average signal ratios, signal-to-noise ratios, and apparent diffusion coefficient (ADC) values in each anatomic region in 25 normal subjects*

Anatomic location	Signal ratios[a]		Signal-to-noise ratios		ADC values ($\times 10^{-4}$ mm^2/s)
	b = 1,000	b = 3,000	b = 1,000	b = 3,000	
Internal capsule	1.20	1.54	28	13	7.0
Frontal white matter	0.85	1.00	20	9	7.9
Cerebral peduncle	0.98	1.17	23	10	7.8
Tegmentum	1.33	1.86	31	16	7.6
Middle cerebellar peduncle	1.15	1.64	27	13	7.2
Thalamus	1.00	1.00	24	9	8.5
Parietal gray matter	1.12	1.08	26	9	8.4
Cerebellar hemisphere	1.26	1.56	29	14	7.3

[a] Normalized to thalamus.

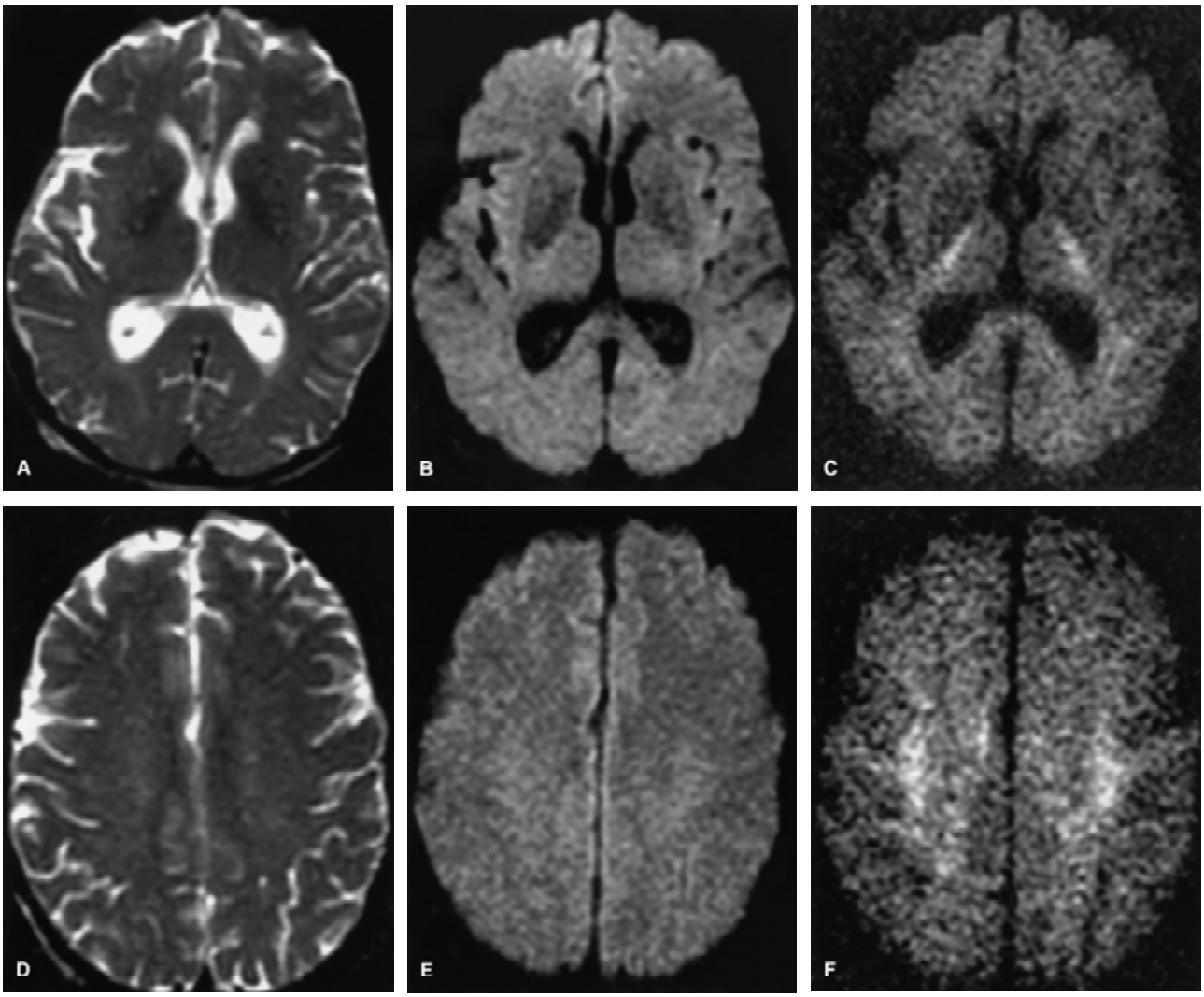

FIG. 1. A 78-year-old woman with history of syncopal episodes has a normal brain MR exam. **A–F:** Diffusion-weighted echo planar images, with A and D acquired at b = 0 s/mm^2, B and E acquired at b = 1,000 s/mm^2, and C and F acquired at b = 3,000 s/mm^2. A–C are the same axial slice at the level of the lateral ventricles, and D–F are at the same level above the lateral ventricles in the region of the centrum semiovale. When b = 3,000 (C and F), the white matter tracts are relatively hyperintense compared with gray matter and the images are noisier than the b = 1,000 images (B and E).

of acute cerebral infarction (4–21). With advancing hardware technology, stronger gradients and faster slew rates have led to higher b values and the ability to obtain images with a much greater degree of diffusion weighting. In this study, we have shown the benefits and limitations of high b-value DW imaging in the normal brain.

Our results can be understood based on several simple and well-established concepts. First, it should be recognized that the MR signal on DW images is a mixture of effects due to spin density, T2, and ADC (the extremely long TR minimizes T1 contributions to signal intensity). The spin density and T2 effects, sometimes called "shine-through," are reduced using higher b values.

Applying a larger diffusion gradient exponentially decreases signal in all structures but to different degrees based on the ADC value within each voxel. Published ranges for typical ADC values (mm^2/s) in the normal brain include the following: CSF = 2.9×10^{-3}–3.0×10^{-3}, gray matter = 8×10^{-4}–10×10^{-4}, and white matter = 2×10^{-4}–10×10^{-4} (24,25). With use of our ADC values for parietal gray matter (8.4×10^{-4}) and internal capsule white matter (7.0×10^{-4}), which are within these published ADC ranges, theoretical signal changes in the gray matter, white matter, and CSF can be calculated at the different b values using the following model (26,27) for MR signal intensity (SI) of the DW imaging sequence:

$$SI = k \cdot SD \cdot e^{-\mathrm{TE/T2}} \cdot e^{-b \cdot \mathrm{ADC}}$$

where k is an arbitrary scaling constant, TE = 97 ms, and SD is spin density. With an increase from b = 1,000 to 3,000, one would expect the signal in parietal gray matter and internal capsule white matter to decrease by

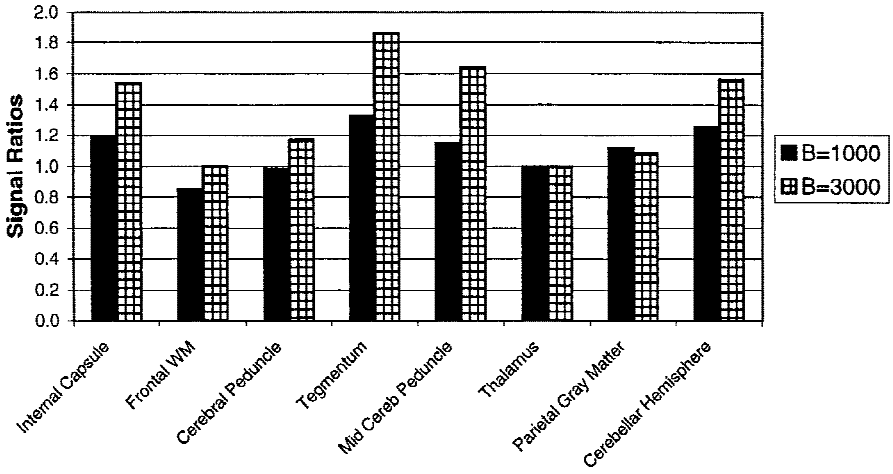

FIG. 2. Bar graph shows the average calculated signal ratios (normalized to thalamus) in eight anatomic regions at b = 1,000 (black bars) and b = 3,000 (shaded bars).

factors of 5.4 and 4.2, respectively. With the lower ADC, white matter signal decreased the least. Thus, the white matter should appear hyperintense compared with gray matter. Our measurements substantiate these conclusions. All white matter structures were relatively more hyperintense on the $b = 3{,}000$ images (Figs. 1 and 2). When analyzing the $b = 3{,}000$ images, it is important to be aware of this relative hyperintensity of the white matter so as not to erroneously diagnose pathology in these regions.

SNR issues become important at higher b-value DW imaging owing to the exponential loss in signal with increasing b value. We purposely kept our parameters the same for the $b = 1{,}000$ and $b = 3{,}000$ images so that SNR comparisons could be easily performed. As shown in Fig. 3, the SNRs were significantly lower in all anatomic structures in the $b = 3{,}000$ images. To maintain equivalent SNR levels between $b = 1{,}000$ and $b = 3{,}000$ brain images, the number of excitations would have to be increased by a factor of 4.7.

In summary, increasing the diffusion gradient from $b = 1{,}000$ to $b = 3{,}000$ creates greater diffusion weighting of the final image but at the expense of a significant reduction in SNR. The appearance of the brain on high b-value DW images is significantly different from low b-value images, with white matter becoming relatively hyperintense and the cortical gray matter becoming so hypointense that anatomic surface landmarks of the brain may be lost.

CONCLUSION

We evaluated the appearance of the normal brain on DW MR images as the diffusion gradient strength (b value) increased from 1,000 to 3,000 s/mm^2 and found that the brain appeared significantly different on DW images as the b value increased. As expected, with increasing b value, both gray and white matter structures exhibited diminished signal based on their ADC values, but given their lower ADC values, the white matter structures appeared relatively hyperintense compared with gray matter on the $b = 3{,}000$ images. In addition, when all other imaging parameters are held constant, at $b = 3{,}000$, the SNRs were significantly lower than at $b = 1{,}000$. Further studies are necessary to determine wheth-

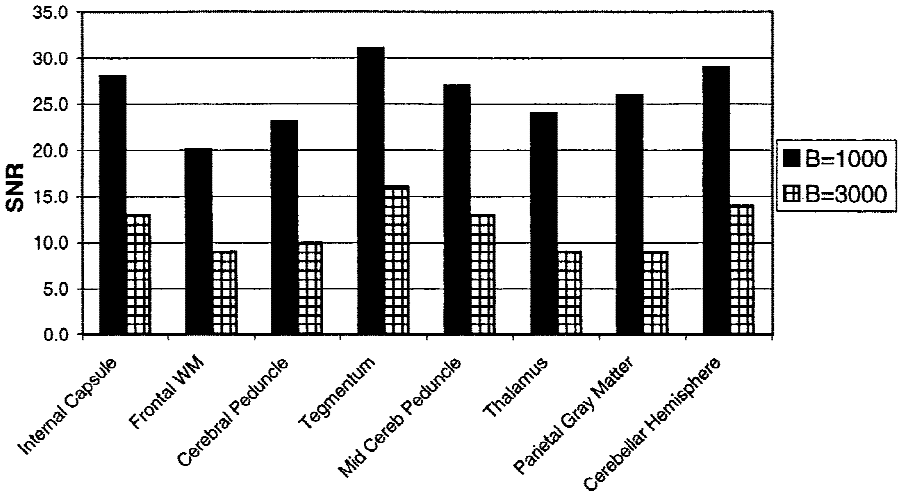

FIG. 3. Bar graph shows signal-to-noise ratios (SNRs) for eight anatomic regions at b = 1,000 (black bars) and b = 3,000 (shaded bars).

er the benefits of this increased diffusion sensitivity at $b = 3{,}000$ are worth the significant loss in SNR (or, equivalently, increased imaging time to maintain SNR), the obscuration of surface landmarks of the brain, and the creation of images where the white matter tracts are significantly hyperintense compared with gray matter structures.

Acknowledgment: The authors thank the MR technologists for their unending patience and support for MR research.

REFERENCES

1. Chien D, Buxton RB, Kwong KK, et al. MR diffusion imaging of the human brain. *J Comput Assist Tomogr* 1990;14:514–20.
2. Burdette JH, Elster AD, Ricci PE. Acute cerebral infarction: quantification of spin-density and T2 shine-through phenomena on diffusion-weighted MR images. *Radiology* 1999;212:333–9.
3. Stejskal EO, Tanner JE. Spin diffusion measurements: spin echoes in the presence of a time-dependent field gradient. *J Chem Phys* 1965;42:288–92.
4. Beauchamp NJ Jr, Barker PB, Wang PY, et al. Imaging of acute cerebral ischemia. *Radiology* 1999;212:307–24.
5. Provenzale JM, Sorensen AG. Diffusion-weighted MR imaging in acute stroke: theoretic considerations and clinical applications. *AJR* 1999;173:1459–67.
6. Kucharczyk J, Mintorovitch J, Asgari HS, et al. Diffusion/perfusion MR imaging of acute cerebral ischemia. *Magn Res Med* 1991;19:311–5.
7. Jones SC, Perez-Trepichio AD, Xue M, et al. Magnetic resonance diffusion-weighted imaging: sensitivity and apparent diffusion constant in stroke. *Acta Neurochir [Suppl] (Wien)* 1994;60: 207–10.
8. Minematsu K, Li L, Sotak CH, et al. Reversible focal ischemic injury demonstrated by diffusion-weighted magnetic resonance imaging in rats. *Stroke* 1992;23:1304–11.
9. Moseley ME, Cohen Y, Mintorovitch J, et al. Early detection of regional cerebral ischemia in cats: comparison of diffusion- and T2-weighted MRI and spectroscopy. *Magn Res Med* 1990;14: 330–46.
10. Mintorovitch J, Moseley ME, Chileuitt L, et al. Comparison of diffusion- and T2-weighted MRI for the early detection of cerebral ischemia and reperfusion in rats. *Magn Res Med* 1991;18:39–50.
11. Warach S, Gaa J, Siewert B, et al. Acute human stroke studied by whole brain echo planar diffusion-weighted magnetic resonance imaging. *Ann Neurol* 1995;37:231–41.
12. Warach S, Dashe JF, Edelman RR. Clinical outcome in ischemic stroke predicted by early diffusion-weighted and perfusion magnetic resonance imaging: a preliminary analysis. *J Cereb Blood Flow Metab* 1996;16:53–9.
13. Sorenson AG, Buonano FS, Gonzalez G, et al. Hyperacute stroke: evaluation with combined multisection diffusion-weighted and hemodynamically weighted echo-planar MR imaging. *Radiology* 1996;199:391–401.
14. Lutsep HL, Albers GW, DeCrespigny A, et al. Clinical utility of diffusion-weighted magnetic resonance imaging in the assessment of ischemic stroke. *Ann Neurol* 1997;41:574–80.
15. Warach S, Chien D, Li W, et al. Fast magnetic resonance diffusion-weighted imaging of acute human stroke. *Neurology* 1992;42: 1717–23.
16. Marks MP, de Crespigny A, Lentz D, et al. Acute and chronic stroke: navigated spin-echo diffusion-weighted MR imaging. *Radiology* 1996;199:403–8.
17. Burdette JB, Ricci PE, Petitti N, et al. Cerebral infarction: time course of signal intensity changes on diffusion-weighted MR images. *AJR* 1998;171:791–5.
18. Le Bihan D, Breton E, Lallemand D, et al. MR imaging of intravoxel incoherent motions: application to diffusion and perfusion in neurologic disorders. *Radiology* 1986;161:401–7.
19. Reith W, Hasegawa Y, Latour LL, et al. Multislice diffusion mapping for three-dimensional evolution of cerebral ischemia in a rat stroke model. *Neurology* 1995;45:172–7.
20. Schlaug G, Siewert B, Benfield A, et al. Time course of the apparent diffusion coefficient (ADC) abnormality in human stroke. *Neurology* 1997;49:113–9.
21. Beauchamp NJ, Bryan RN. Acute cerebral ischemic infarction: a pathophysiologic review and radiologic perspective. *AJR* 1998; 171:73–84.
22. Burdette JH, Elster AD, Ricci PE. Calculation of apparent diffusion coefficients (ADCs) in brain using two-point and six-point methods. *J Comput Assist Tomogr* 1998;22:792–4.
23. Xing D, Papadakis NG, Huang CLH, et al. Optimised diffusion-weighting for measurement of apparent diffusion coefficient (ADC) in human brain. *Magn Res Imag* 1997;15:771–84.
24. Le Bihan D, Turner R, Douek P, et al. Diffusion MR imaging: clinical applications. *AJR* 1992;159:591–9.
25. Sorenson AG, Rosen BR. Functional MRI of the brain. In: Atlas SW, ed. *Magnetic Resonance Imaging of the Brain and Spine. 2nd Ed.* Philadelphia: Lippincott–Raven Publishers, 1996:1501–45.
26. Kjos BO, Ehman RL, Brant-Zawadzki M, et al. Reproducibility of relaxation times and spin density calculated from routine MR imaging sequences: clinical study of the CNS. *AJR* 1985;144: 1165–70.
27. Breger RK, Wehrli FW, Charles HC, et al. Reproducibility of relaxation and spin-density parameters in phantoms and the human brain measured by MR imaging at 1.5 T. *Magn Res Med* 1986;3: 649–62.